ACS OMEGA

Open Access

http://pubs.acs.org/journal/acsodf

Article

Biosynthesis of TiO_2/CuO and Its Application for the Photocatalytic Removal of the Methylene Blue Dye

Getye Behailu Yitagesu, Dereje Tsegaye Leku,* Abebaw Matebu Seyume, and Getachew Adam Workneh*

Cite This: *ACS Omega* 2024, 9, 41301−41313

Read Online

ACCESS | Metrics & More | Article Recommendations | Supporting Information

ABSTRACT: In this study, we successfully synthesized a TiO_2/CuO nanocomposite using the aqueous extract of *Impatiens tinctoria A.rich.* leaf extract as a capping, reducing, and stabilizing agent for the first time in an environmentally friendly, low-cost, straightforward, and sustainable technique. Numerous characterization techniques such as ultraviolet−visible diffuse reflectance spectroscopy (UV−vis-DRS), photoluminescence (PL), Raman spectroscopy, Fourier-transform infrared (FTIR), energy dispersive X-ray (EDX), transmission electron microscopy (TEM), X-ray diffraction (XRD), scanning electron microscopy (SEM), Brunauer−Emmett−Teller (BET), and high resolution TEM (HRTEM) were used to characterize the obtained TiO_2/CuO nanocomposite. XRD verified that the TiO_2/CuO nanocomposite has an average crystallite size of about 21 nm. The TEM result revealed an average particle size of 29 nm for the biosynthesized TiO_2/CuO NC. The HRTEM analysis showed the presence of polycrystalline structures with the predominant lattice fringes 0.352 and 0.19 which were attributed to anatase phase TiO_2 in the crystal plane of (101) and (200), respectively. The lattice fringes for monoclinic CuO were observed with values of 0.213 and 0.252 for the lattice planes of (111) and ($11\bar{1}$), respectively. The photoluminescence spectroscopic analysis revealed that the TiO_2/CuO NC showed the lowest intensity compared to the pristine TiO_2 and CuO indicating the reduction of exciton recombination in the case of the TiO_2/CuO NC. The BET analysis showcased the formation of mesoporous materials with a surface area of 87.5 m^2/g. The photocatalytic degradation performance of the biosynthesized TiO_2, CuO, and TiO_2/CuO nanomaterials against the potentially harmful MB dye was tested using the light source of a 150 tungsten-halogen lamp with a wavelength range of 360−2800 nm. The factors affecting photodegradation efficiencies like catalyst dose (20 mg), dye concentration(15 ppm), pH (9), and reaction time (90 min) were optimized for the degradation of the MB dye. The TiO_2/CuO catalyst showed the highest degradation efficiency of 99% under the optimized conditions. The degradation rate of the MB dye in the presence of the TiO_2/CuO NC was evaluated and found to be fitted to the pseudo-first-order kinetics with a rate constant of 0.03 min^{-1}. The reusability test of the TiO_2/CuO catalyst showed its good stability.

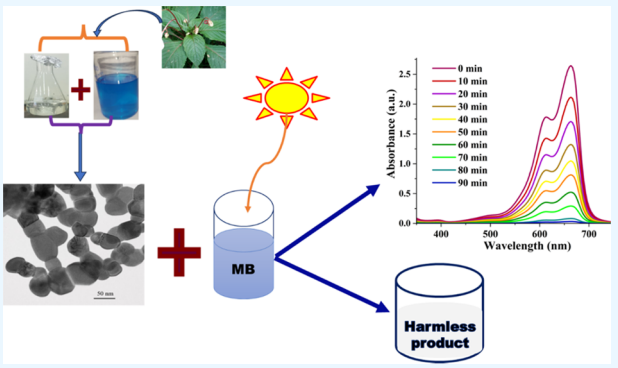

1. INTRODUCTION

Water is one of the most important elements of human existence. It is essential to our physical existence and the most basic requirement for life. Water is needed for many household and commercial tasks, including cooking, cleaning, gardening, and manufacturing.[1] Globally, concerns over the availability of clean water are becoming more and more connected to environmental and health issues. Pollutants like organic dyes can leak into aquatic habitats, which is one of the unintended effects of many new industries and technology.[2−5] These toxic organic dyes are among the many pollutants that have contaminated water in recent years due to the increased demand for contemporary technologies.[6,7] Ingestion of organic dyes has been linked to several health problems in humans, including vomiting, gastritis, irregular heartbeat, chest pain, and excessive perspiration, according to numerous researches.[8,9] Among those water-soluble cationic dyes, methylene blue has a low biodegradability. This causes the dye to stay in the environment for a long time, ruining natural ecosystems.[10,11] As a result, numerous approaches, such as adsorption, membrane separation,[12] ultrafiltration,[13] ion exchange,[14] and photocatalysis[15] have been developed to remove methylene blue from polluted water. Among them, the elimination of long-lasting contaminants and the production of safe end products can be achieved by heterogeneous

Received: April 10, 2024
Revised: September 6, 2024
Accepted: September 10, 2024
Published: September 24, 2024

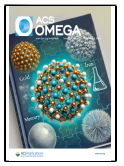

photocatalysis, which makes use of semiconductor materials and a variety of light sources.[16] A positive hole (h^+) is created in the valence band of a semiconductor during the photocatalytic process when an electron (e^-) is excited from the valence band (VB) to the conduction band (CB) in the presence of light with an energy higher than the corresponding band gap of the material.[17] The process of photocatalytic degradation is started by the photogeneration of charge carriers (e^-/h^+).[18] In photocatalytic degradation, nanomaterials play a great role in the efficient removal of pollutants. Since nanotechnology is so versatile and has so many uses in nearly every scientific field, it has received more attention. The main focus of nanotechnology is on the supermolecule scale of atoms and molecules.[19,20] At this stage, the physicochemical properties of nanomaterials drastically altered because of the increasing surface area-to-volume ratio. In addition to its size, structure, physicochemical properties, and biological traits, nanotechnology offers a wide range of uses in many different industries, including molecular diagnostics, mechanical, electrical, and imaging-specific targeting. On an ongoing basis, the application of nanomaterials is extended in the fields of medicine, cosmetics, pharmaceuticals, and energy development.[21,22]

Metal oxide nanomaterials, such as ZnO,[23] Nb_2O_5,[24] SnO_2,[25] CuO,[26] CeO_2,[27] $BiVO_4$,[28] WO_3,[29] Fe_2O_3,[30] TiO_2,[31] and In_2O_3[32] are used in different applications because of their fascinating thermal, optical, electrical, and magnetic properties. Building a heterojunction that can, in comparison to single metal oxide nanomaterials, increase the surface area-to volume ratio and minimize the recombination of electron/hole pairs is important because of the synergistic effect. One can use metal oxides with the same band gap or different band gaps to generate the heterojunction.[33−35] The synthesis of these nanomaterials can be classified as chemical,[36,37] physical,[38] and biological methods.[39] Conventional synthesis processes, encompassing both chemical and physical methods, are typically executed in exceedingly severe environments. The biological processes, on the other hand, are typically carried out at room temperature and pressure, indicating simplicity, energy efficiency, and a decreased risk of toxicity or harm to both people and the environment.[40] The objective of green synthesis is to advance revolutionary technologies that minimize the need for dangerous materials in the creation, production, and usage of chemical products. This entails minimizing or, if at all feasible, completely removing the pollution generated during the synthesis processes, refraining from releasing hazardous substances in the production of materials, and reducing the time needed for synthesis.[41]

So far, there is no scientific report on the characterization and biological activities of TiO_2/CuO materials synthesized by *Impatiens tinctoria* A.Rich leaves extract. The objective of the present study was to successfully investigate the photocatalytic activities of TiO_2/CuO nanocomposites prepared by using *I. tinctoria* A.Rich leaf extract.[42] *I. tinctoria* A.Rich is a member of the Balsaminaceae family. It thrives near streams and shaded banks, along woodland edges and gullies, and in wet, dark places in upland rainy woods.[43] Ethiopians have long used the impatiens tinctoria tuber as a traditional folk remedy for various ailments. Chewing the stem can cure bacterial and fungal diseases in the mouth and throat and treat wounds aseptically. Its root infusion is drunk as a laxative also to treat pain in the abdomen.[44] The fact that Impatiens tinctoria tubers are traditionally used for hand toughening is evidence of their abundance in bioactive antiaging chemical substances. Additionally, recent research revealed that the tuber of Impatiens tinctoria is a rich source of several secondary metabolites.[45]

The biosynthesized TiO_2/CuO NC synthesized using *I. tinctoria* A.Rich leaves extract for the photodegradation of methylene blue (MB) with a surface area of 87.5 m^2/g showed a good mesoporous behavior. The scanning electron microscopy (SEM) and transmission electron microscopy (TEM) morphology also showed nearly homogeneous nanoparticles (NPs) with reduced agglomeration, which is related to the extract of *I. tinctoria* A.Rich leaves having the ability to cap during synthesis. As a result, this mesoporous structure may help to increase TiO_2/CuO NC's photocatalytic activity of the MB dye. There are many advantages to the green synthesis method, which uses plant extract from *I. tinctoria* A.Rich leaves as a stabilizing and reducing agent. The low toxicity of the resultant nanomaterials has a major advantage since plant extract can substitute harsh chemical reagents, making the formation of safer nanocomposites for the environment and human health possible. Green synthesis also reduces the amount of hazardous waste produced and the environmental damage caused by nanomaterial synthesis, which is in line with ecofriendly and sustainable methods.

2. EXPERIMENTAL SECTION

2.1. Materials and Methods. The materials used in this work were copper nitrate hexahydrate (Luba India, 96%), titanium tetra isopropoxide (TTIP, 97.5%, Merck, Germany), ethanol (99.9%, Luba, India), hydrochloric acid (HCl) (SRL, 37%), deionized water, sodium hydroxide (98%, Luba, India), methylene blue ($C_{16}H_{18}ClN_3S$, Dallul Pharmaceuticals plc), and *I. tinctoria* A.Rich leaves. All of the reagents were analytical grade and used as received without further purification.

2.2. Extraction of Plant Leaves. The extraction was carried out using the technique described by Basit and colleagues with modifications.[46] First, *I. tinctoria* A.Rich leaves were collected from the Menz Gera Midir, Amhara regional state, Ethiopia. The collected leaves were thoroughly cleaned using tap water and distilled water to remove dirt. Now, leaves were allowed to air-dry at room temperature in the dark for 2 weeks. These dry leaves were then ground in a lab grinder to produce a powder. To prepare leaf extract, which was to be employed as a capping/stabilizing agent, 20 g of powder was added to 200 mL of deionized water, and the combination was heated to 60 °C with stirring magnetically for 1 h. After being heated, the extract was filtered through the Whatman filter (shown in Figure S1).

2.3. Biosynthesis of Photocatalysts. To synthesize TiO_2, 15 mL of TTIP solution was mixed with 50 mL of *I. tinctoria* A.Rich leaves extract and continuously stirred at room temperature for 12 h. TiO_2 NPs were formed after calcination at 400 °C for 3 h. The same procedure was followed to synthesize the CuO NPs. To synthesize the TiO_2/CuO NC, an amount of 15 mL of TTIP solution was added to 100 mL of *I. tinctoria* A.Rich leaves extract followed by the addition of 15 mL of 0.2 mM $Cu(NO_3)_2{\cdot}6H_2O$. Then the mixture was stirred magnetically for 12 h and filtered using the Whatman filter paper. The biosynthesized nanocomposite was calcined at 400 °C for 3 h.

2.4. Characterization of the Biosynthesized Nanomaterials. Several characterization approaches were used to examine the properties of the biosynthesized nanomaterials. The X-ray diffraction (XRD) study was performed on a

https://doi.org/10.1021/acsomega.4c03472
ACS Omega 2024, 9, 41301−41313

Shimadzu 7000 X-ray diffractometer (Japan) equipped with a Cu Kα1 radiation source (λ = 1.5406 Å) with an accelerating voltage of 40 kV and a source current of 30 mA at a scanning rate of 4° min^{-1} in 2θ range of 10−80°. By analyzing nitrogen adsorption−desorption at 77.7 K with an instrument called the Quantachrome v11.02, USA, the Brunauer−Emmett−Teller (BET) study of pore size, specific surface area distribution, and pore volume was assessed.

The Raman spectrometer (JASCO, NRS-5000, Japan) was used to evaluate the Raman spectrum. The ultraviolet−visible (UV−vis) defused reflectance spectrophotometer (JASCO V-750 UV−vis) has been utilized to measure the UV−vis-diffused reflectance spectra. Fourier-transform infrared (FTIR) spectra were obtained using an FTIR-6600 spectrometer (JACO International Co., Ltd., Tokyo, Japan) between 4000 and 400 cm^{-1}. An UV−vis spectrophotometer was used to study the degradation of the MB dye. The morphology of biosynthesized structures was examined using a SEM technique (400, FEG). Energy-dispersive X-ray spectroscopy was utilized to examine the elemental composition. A transmission electron microscope (FEI, Titan, 80−300 kV) operated at 300 kV was used to produce exceptionally detailed lattice images.

2.5. Photocatalytic Performance Test. The photocatalytic degradation activities of TiO_2, CuO, and TiO_2/CuO against the MB dye were studied under a 150 W tungsten-halogen lamp (Philips, China) with a wavelength range of 360−2800 nm. An amount of 100 mL aqueous solutions of the methylene blue dye (5−30 ppm) were prepared in vessels and an appropriate amount of TiO_2, CuO, and TiO_2/CuO catalysts (10−40 mg) were added. To ensure sufficient adsorption−desorption equilibrium, the solutions were sonicated in the dark for 30 min before being exposed to light. An amount of 4 mL of the MB dye solution was extracted from the reaction mixture every 10 min, and the UV−vis spectrophotometer was used to measure the absorbance. The percentage of removal of the MB dye by the catalysts was evaluated using the formula in eq 1.[46]

$$\%\text{degradation} = \frac{A_o - A}{A_o} \times 100 \tag{1}$$

where A_0 is absorbance, before irradiation, and the parameter A is its absorbance, at any time t after the irradiation has started.

3. RESULTS AND DISCUSSION

3.1. X-ray Diffraction Analysis. The XRD patterns of biosynthesized TiO_2, CuO, and TiO_2/CuO nanomaterials are indicated in Figure 1. The TiO_2 was identified by the characteristic diffraction peaks at 25.28° (101), 36.75° (103), 37.81° (004), 48.04° (200), 53.79° (105), 55.15° (211), 62.81° (204), 68.78° (116), 70.45° (220), and 75.13° (215) which correspond to the anatase phase of titanium dioxide (JCPDS #21−1272).[47] The characteristic diffraction peaks of copper oxide and the accompanying 2θ at 32.52° (110), 35.65° ($11\bar{1}$), 38.84° (111), 48.94° ($20\bar{2}$), 53.72° (020), 61.63°($11\bar{3}$), and 66.42° ($31\bar{1}$) suggest the formation of CuO and match with the standard JCPDS reference #48−1548.[48] The presence of the major peaks of both components clearly shows the formation of the TiO_2/CuO nanocomposite.

The average crystallite size was calculated using Scherrer's equation (eq 2).

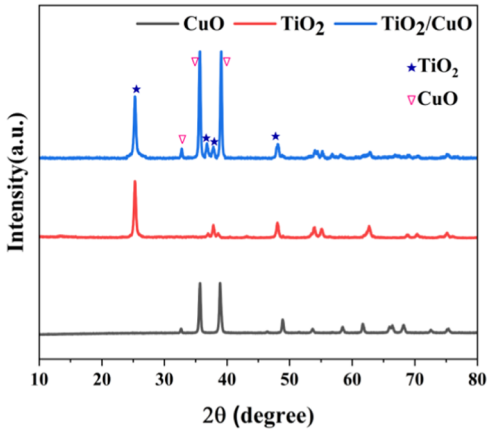

Figure 1. X-ray diffraction of biosynthesized TiO_2/CuO, TiO_2, and CuO nanomaterials.

$$D = \frac{k\lambda}{\beta \cos \theta} \tag{2}$$

where D represents the average crystallite size (nm), k is Scherrer's constant, λ represents the wavelength of the X-ray Cu Kα source (1.5406 Å), and β denotes the full width at half-maximum (fwhm) of the X-ray diffraction peak which appears at 2θ.

The average crystallite sizes of the biosynthesized photocatalysts were found to be 14, 17, and 21 nm for TiO_2, CuO, and TiO_2/CuO, respectively.

3.2. UV−Vis-DRS Analysis of Biosynthesized Nanomaterials. The UV−vis-diffused reflectance spectra of the biosynthesized TiO_2, CuO, and TiO_2/CuO are displayed in Figure 2A. The band gap energy of synthesized materials was calculated using the Tauc plots method as expressed in eq 3.[49,50]

$$(F(R)\cdot h\nu)^{1/n} = A(h\nu - E_g) \tag{3}$$

where $F(R)$ is the Kubelka−Munk function, which is expressed in eq 4, h is Planck's constant, and the exponent n depends on the type of the electron transition (n = 2 direct and n = 1/2 indirect transitions, respectively), A is a constant, ν is the frequency of light energy, and E_g = band gap energy.

$$F(R) = \frac{K}{S} = \frac{(1 - R)^2}{2R} \tag{4}$$

where R, K, and S are reflectance, absorption coefficient, and scattering coefficient, respectively.

Figure 2B displays the Tauc plot of the biosynthesized TiO_2, CuO, and TiO_2/CuO. The band gap energies were estimated from the linear portion extrapolation and found to be 3.23, 1.83, and 2.65 eV for TiO_2, CuO, and TiO_2/CuO, respectively.

It is suggested that a p−n heterojunction forms when n−type and p−type semiconductors are combined to produce an internal electric field in TiO_2/CuO NC. Additionally, the band alignment between TiO_2 and CuO and the creation of this p-n heterojunction significantly aid in electron−hole separation and boost photocatalytic activity by reducing the recombination rate.[51]

3.3. Photoluminescence and FTIR Spectra Analysis. The lifetime of photogenerated electron holes in semiconductors and the effectiveness of charge carrier transfer were both studied by using photoluminescence (PL) emission

https://doi.org/10.1021/acsomega.4c03472
ACS Omega 2024, 9, 41301−41313

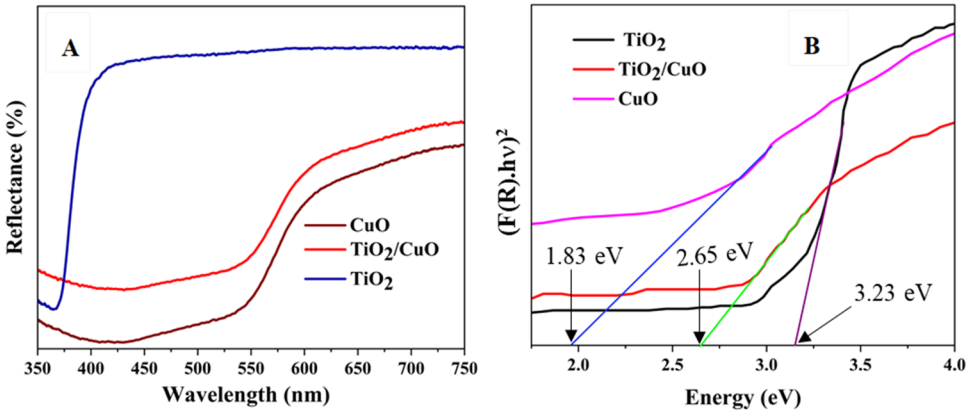

Figure 2. UV−vis-DRS spectra (A), Tauc plot (B) of biosynthesized TiO_2, CuO, and TiO_2/CuO nanomaterials.

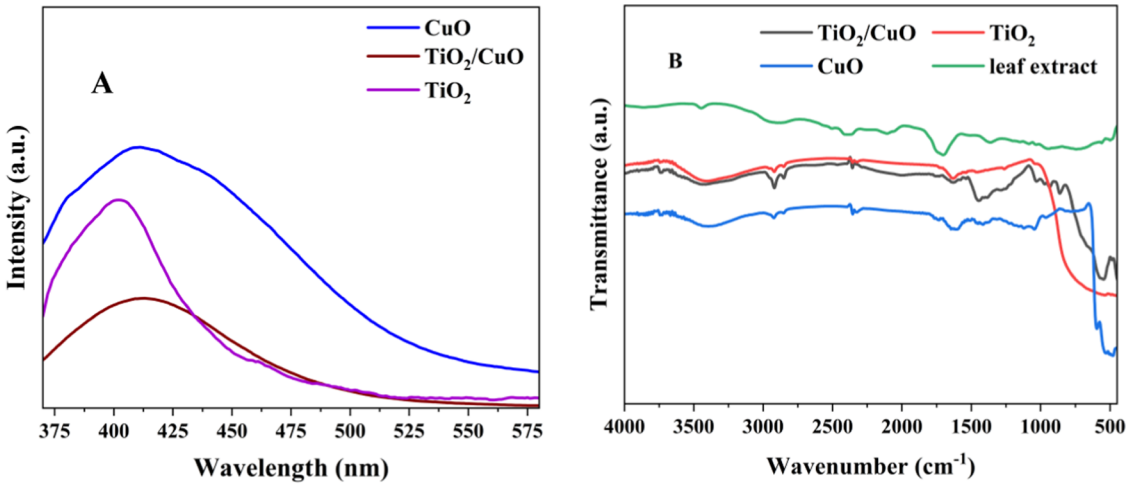

Figure 3. PL spectra (A) of biosynthesized TiO_2, CuO, and TiO_2/CuO nanomaterials and FTIR spectra (B) of biosynthesized TiO_2, CuO, TiO_2/CuO nanomaterials, and plant extract.

spectra. PL spectra were also used in several investigations that showed a notable improvement in the separation of photogenerated carriers as shown in Figure 3A. The TiO_2/CuO is represented by the lowest peak intensity, indicating that the holes and electrons recombination is reduced in the TiO_2/CuO heterostructures as compared to the individual TiO_2 and CuO. The decreased electron−hole recombination improves the photocatalytic effectiveness of TiO_2/CuO NC.[52]

Figure 3B presents the FTIR spectra of TiO_2, CuO, and TiO_2/CuO nanocomposite photocatalysts. The FTIR absorption peaks around 3400 and 1630 cm^{-1} are attributed to the stretching vibrations of surface water molecules, including hydroxyl groups and molecular water on the nanomaterials. The peaks at 493 and 1024 cm^{-1} were ascribed to the stretching modes of Ti−O and Ti−O−Ti bridging.[53] The FTIR spectra of CuO reveal prominent absorption bands between 400 and 600 cm^{-1}. This band indicates the formation of CuO at 529 cm^{-1} and is attributed to the stretching vibration of the Ti−O−Ti bond.[52,54] The FTIR analysis of the plant extract also revealed that the peak at about 3341 cm^{-1} is attributed to the presence of the O−H stretching. The band at about 2923 cm^{-1} corresponds to the C−H stretching. The absorption peak at 1637 cm^{-1} depicts the C═O double bond stretching.[55]

3.4. Morphological Analysis. A SEM analysis was used to assess the biosynthesized TiO_2/CuO NC topological characteristics. The somewhat spherical-like morphology of the NPs generated using *I. tinctoria A.rich* leaf extract is shown in the SEM micrograph in Figure 4A and less agglomeration was noticed in the biosynthesized TiO_2/CuO NC. The presence of distinct phytochemicals (such as flavonoids, terpenoids, polyphenols, and alkaloids) in the plant extract are the components that contribute to the fine morphology of NCs. These phytochemicals interact with metal precursors in different ways, which affect the nucleation and development of TiO_2/CuO NC. The variety of antioxidant kinds and types found in plant extracts can influence the reduction mechanism of the metal precursor during NP synthesis because the extract's various constituents have varying capacities to reduce metal ions and stabilize the formed NC.

The energy dispersive X-ray spectroscopy (EDX) spectra in Figure 4B indicate the presence of Cu, Ti, and O elements in the biosynthesized TiO_2/CuO nanocomposite. The weight percentage of pure TiO_2 was found in Ti (45.57 wt %), O (33.02 wt %), and Cu (21.41 wt %). The percentage atomic values of Ti, Cu, and O were 28.39, 10.06, and 61.55 atom %, respectively, for the TiO_2/CuO nanocomposite. This suggests that the biosynthesized TiO_2/CuO nanocomposite is free of impurities.

In the TEM micrograph (Figure 4C), several pores in TiO_2/CuO NC are observed. The presence of nanopores is known to be beneficial because they increase surface permeability and

https://doi.org/10.1021/acsomega.4c03472
ACS Omega 2024, 9, 41301−41313

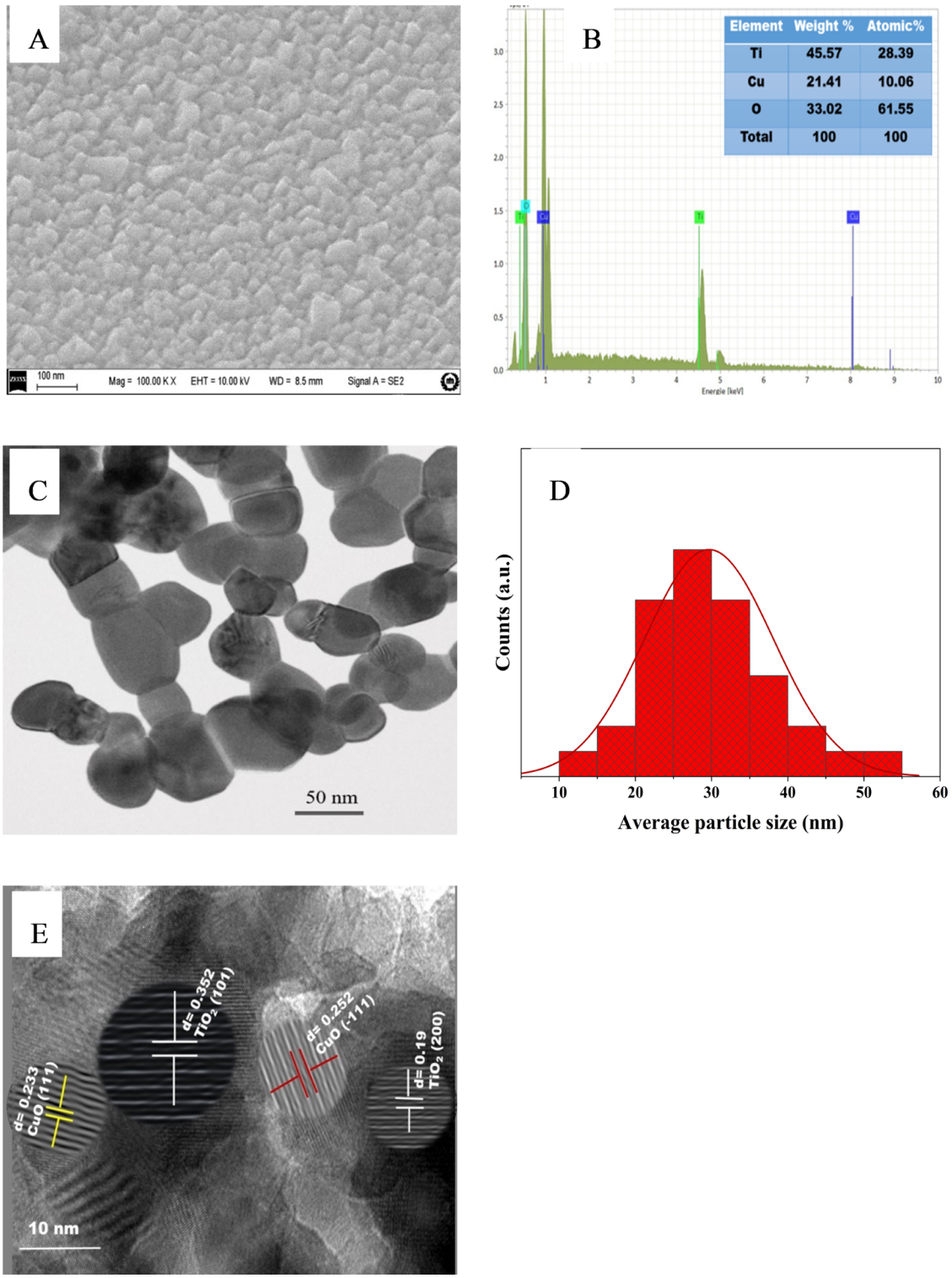

Figure 4. (A) SEM, (B) EDX, (C) TEM (D) particle size distribution histogram from TEM, and (E) HRTEM for the biosynthesized TiO_2/CuO nanocomposite.

improve adsorption efficiency. It is believed to efficiently lower the charge carriers recombination rate and speed up photocatalytic processes, it also permits the quick transport of light-excited charge carriers to the particle surface. The average particle size calculated from the TEM micrograph was 29 nm, as shown in Figure 4D. To determine more about the atomic arrangement and structural characteristics of biosynthesized TiO_2/CuO, a high resolution TEM (HRTEM) image was taken. Figure 4E shows the HRTEM micrograph of TiO_2/CuO. The lattice fringe values of TiO_2 were 0.352 and 0.19 nm for the (101) and (200) planes, respectively. The lattice fringe values of CuO were 0.252 and 0.233 nm for the $(11\bar{1})$ and (111) planes, respectively. These findings provide additional evidence that the composite catalyst contains CuO and TiO_2 nanostructures.

https://doi.org/10.1021/acsomega.4c03472
ACS Omega 2024, 9, 41301−41313

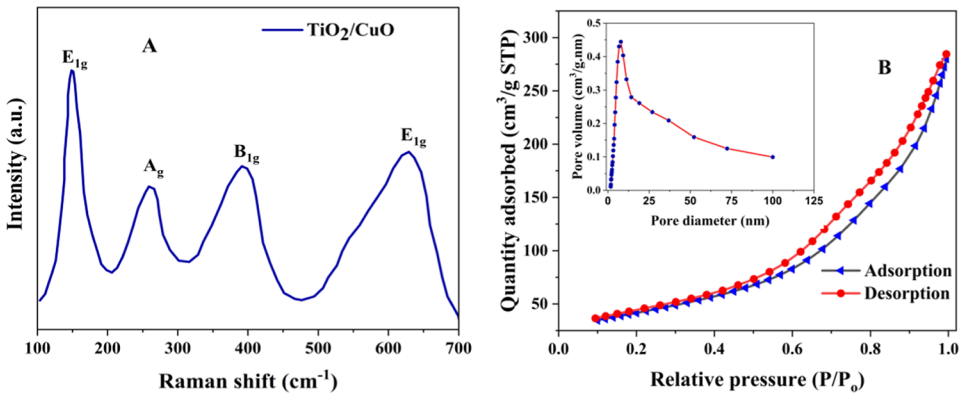

Figure 5. Raman shift spectrum (A) and BET (B) of the biosynthesized TiO_2/CuO NC.

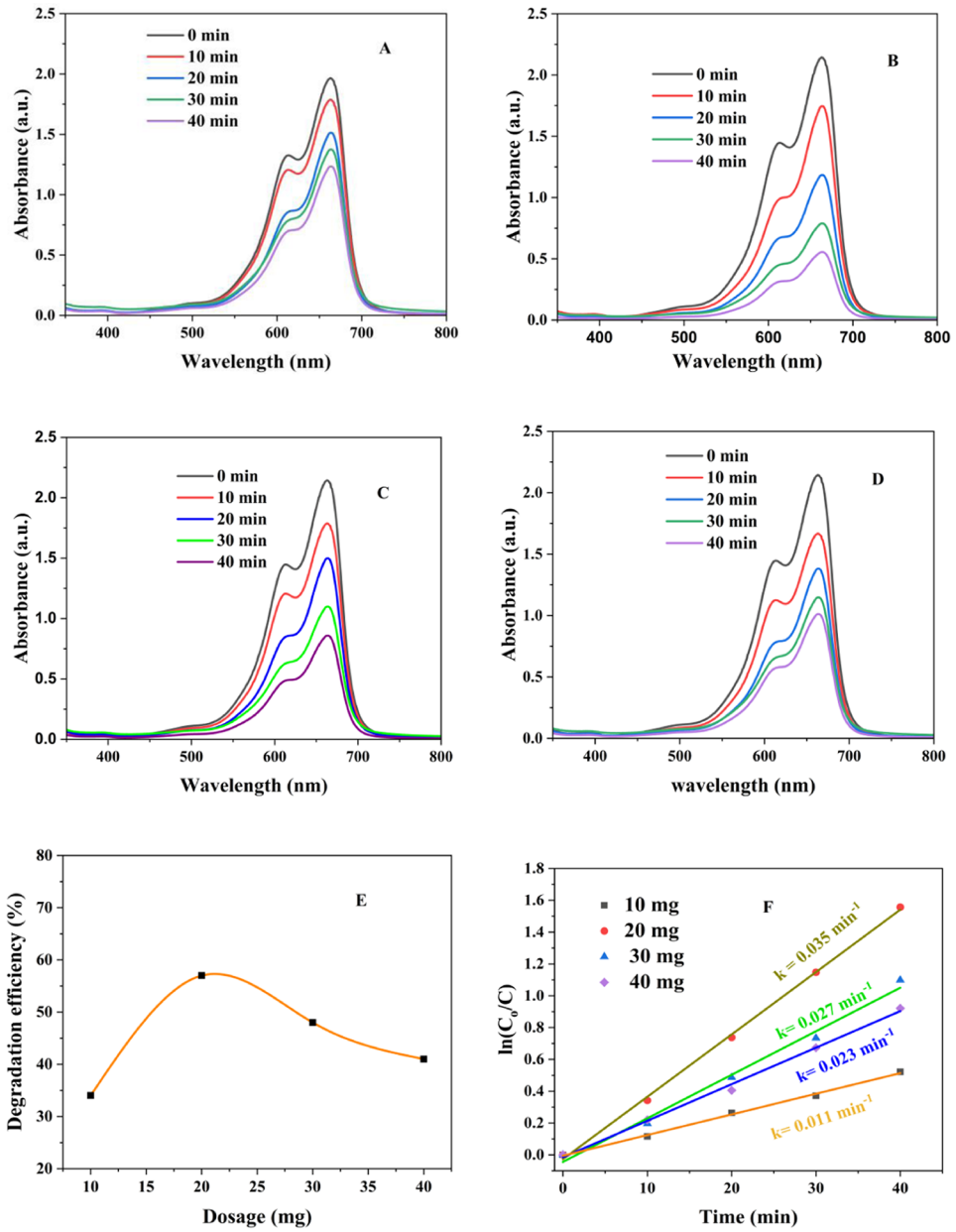

Figure 6. UV−vis absorption spectra of (A) 10 mg, (B) 20 mg, (C) 30 mg, (D) 40 mg, and (E) degradation efficiency of biosynthesized TiO_2/CuO; (F) pseudo-first-order model plots of (A−D).

https://doi.org/10.1021/acsomega.4c03472
ACS Omega 2024, 9, 41301−41313

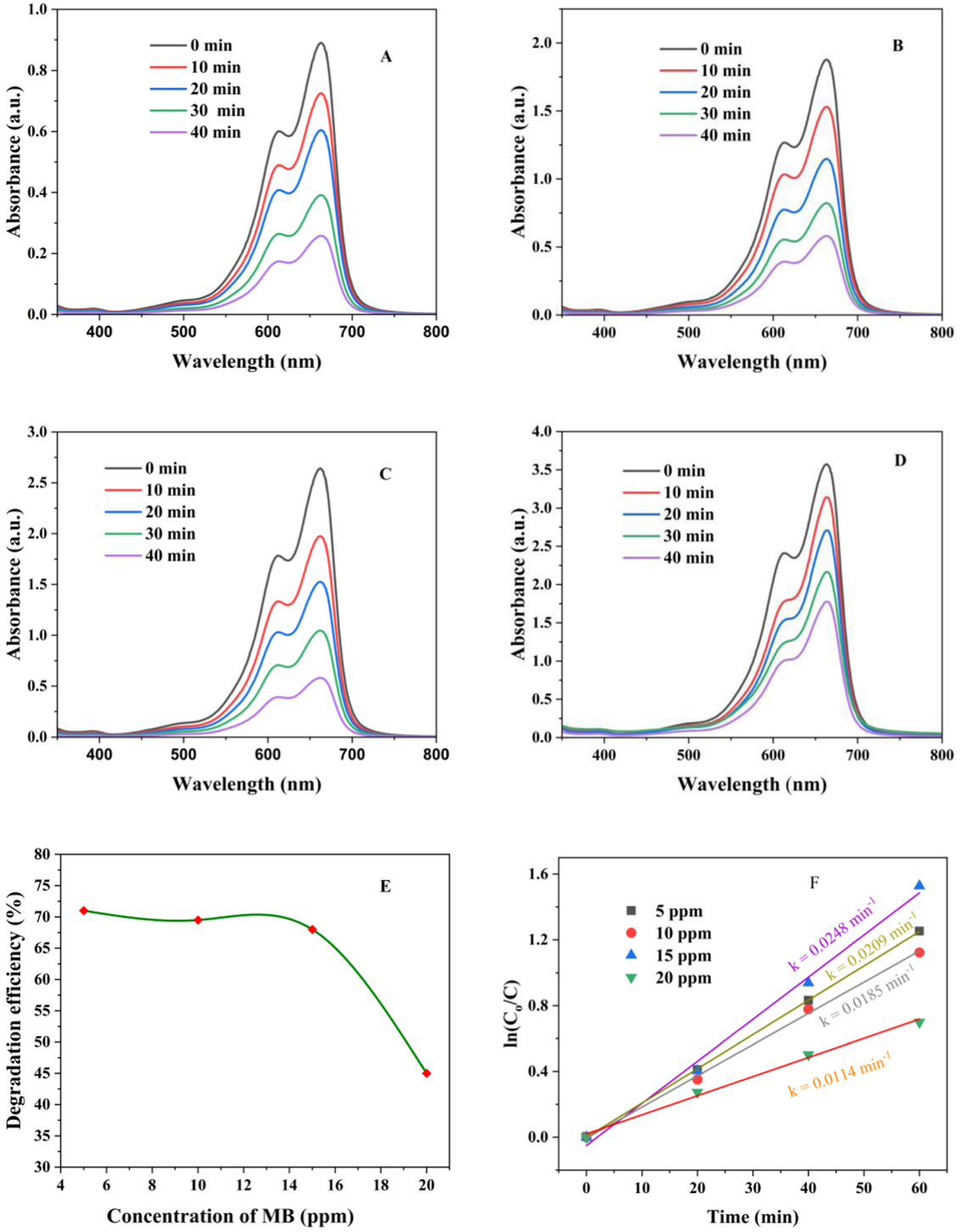

Figure 7. UV−vis absorption spectra of (A) 5 ppm, (B) 10 ppm, (C) 15 ppm, (D) 20 ppm, (E) percent degradation efficiency of biosynthesized TiO_2/CuO NC, and (F) pseudo-first-order model plots of (A−D).

3.5. Raman and BET Analysis. Raman spectroscopy is a widely used technique to analyze the vibrational properties of nanomaterials. Raman spectra of the biosynthesized TiO_2/CuO NC are displayed in Figure 5A. The Raman spectra showed three modes of vibration E_{1g} (147 cm^{-1}), B_{1g} (399 cm^{-1}), and E_{1g} (639 cm^{-1}) which belongs to anatase TiO_2 and one vibrational mode at A_g (268 cm^{-1}) in which monoclinic CuO can be assigned.[56]

The Brunauer−Emmett−Teller (BET) surface area analyzer was used to measure the surface area of the biosynthesized TiO_2/CuO NC. Figure 5B displays the TiO_2/CuO NC loop of the nitrogen adsorption−desorption isotherm. The hysteresis loop belongs to the type IV isotherm. The surface area, pore volume, and average pore diameter of TiO_2/CuO NC were 87.5 m^2/g, 0.083 cm^3/g, and 9.7 nm, respectively. TiO_2/CuO NC showed average pore diameter and surface area which could be accredited for the enhancement of the photodegradation of the methylene blue dye from aqueous solution.[3,48,53]

https://doi.org/10.1021/acsomega.4c03472
ACS Omega 2024, 9, 41301−41313

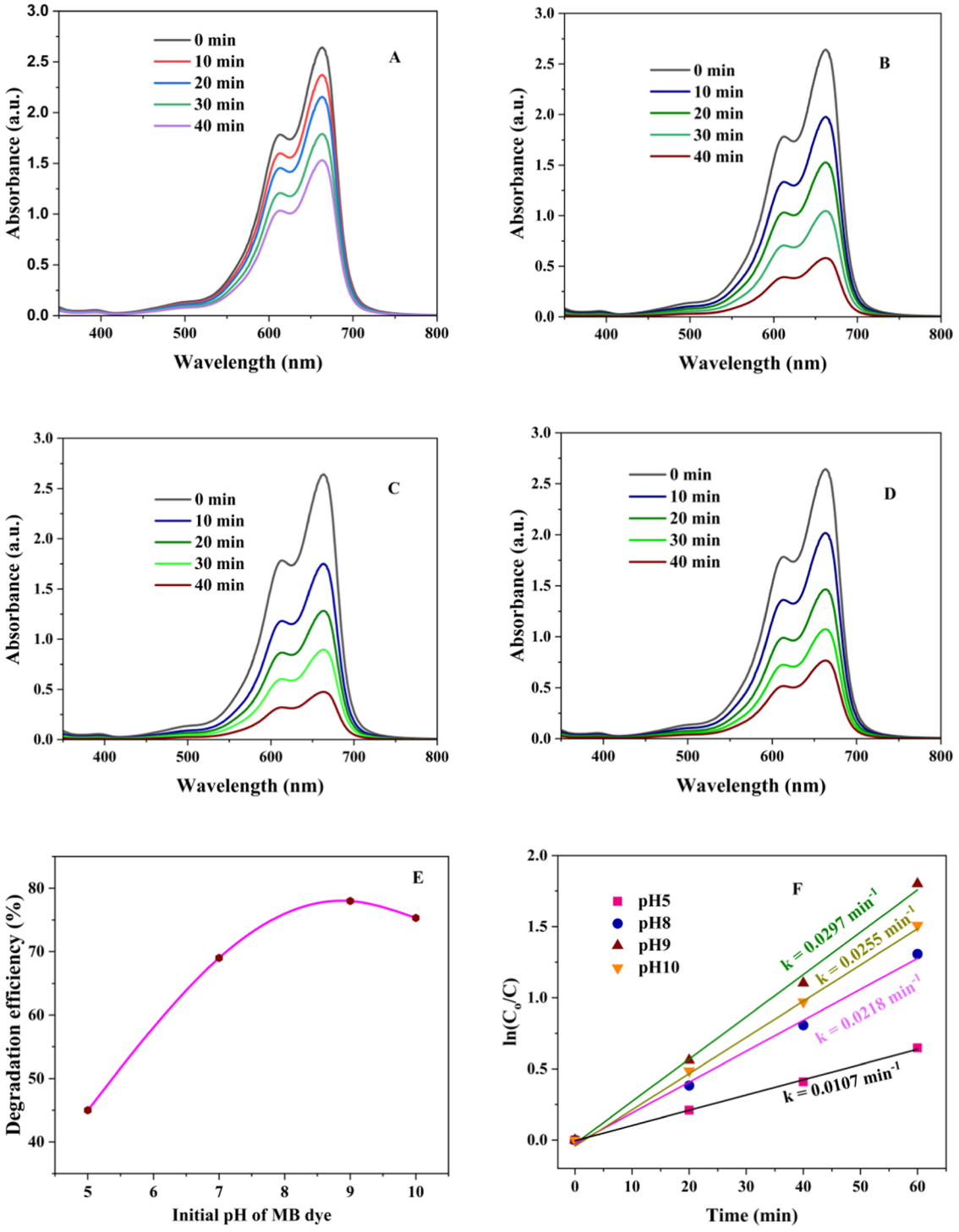

Figure 8. UV−vis absorption spectra of MB at (A) pH5, (B) pH8, (C) pH9, (D) pH10, (E) degradation efficiency of biosynthesized TiO_2/CuO NC, and (F) pseudo-first-order model plots of (A−D).

3.6. Photocatalytic Performance of TiO_2, CuO, and TiO_2/CuO Nanomaterials. The photocatalytic degradation of the MB dye solution by the TiO_2, CuO, and TiO_2/CuO NC was evaluated under light irradiation. TiO_2, CuO, and TiO_2/CuO were tested as photocatalysts in an aqueous MB dye. Factors affecting the efficiency of photocatalysis were optimized and discussed in the following subtopics.

3.6.1. Effect of Dosage. The impact of catalyst dosage on the breakdown of 10 ppm MB solution is depicted in Figure 6A−F. It was shown that the percentage of photodegradation rose as catalyst dosage increased up to the optimum (20 mg) at the MB dye concentration of 10 ppm, at pH 8 for 40 min of light irradiation. The degradation efficiency decreased as the catalyst dosage was increased above 20 mg. The first increase in the percentage of degradation may have been caused by an increase in the number of active sites on the TiO_2/CuO surface brought on by a higher TiO_2/CuO dosage. The quantity of free radicals such as $OH^{\bullet}$ and O_2^{2-} in solution increases when the TiO_2/CuO dosage is increased, which in turn promotes improved photodegradation of the MB dye. The

https://doi.org/10.1021/acsomega.4c03472
ACS Omega 2024, 9, 41301−41313

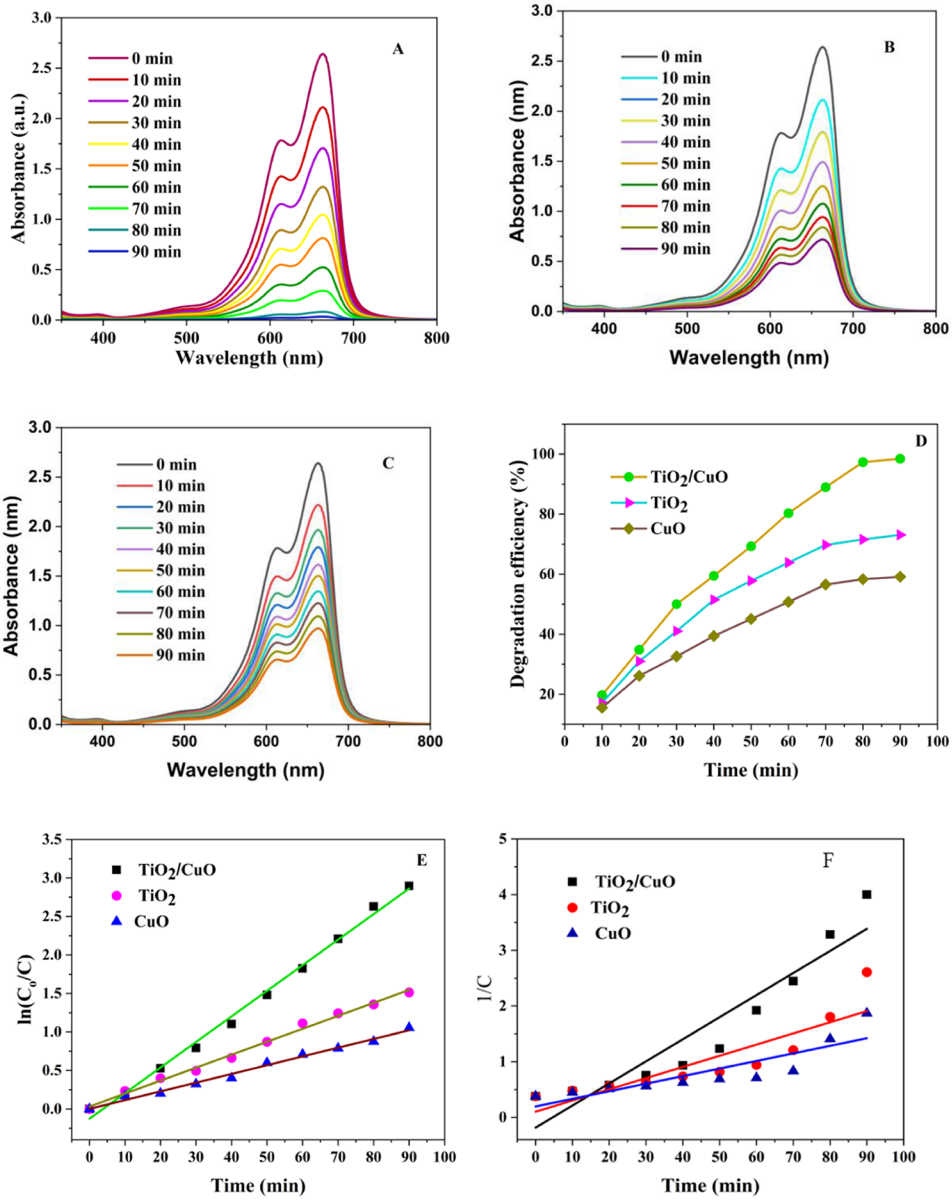

Figure 9. UV−vis absorption spectra of biosynthesized (A) TiO_2/CuO, (B) TiO_2, (C) CuO, (D) degradation efficiency of biosynthesized TiO_2/CuO, TiO_2, and CuO; (E) pseudo-first order model plots of TiO_2/CuO, TiO_2, and CuO and (F) pseudo-second-order model plots of TiO_2/CuO, TiO_2, and CuO.

subsequent decline in photodegradation can be easily explained by the fact that when the catalyst dosage is increased beyond the optimal level, the suspended TiO_2/CuO NC aggregate. This lowers the amount of light that reaches the surface photocatalyst active sites, which lowers the rate of degradation.[57]

3.6.2. Effect of Initial Dye Concentration. One of the most important factors in wastewater treatment is the concentration of pollutants. The starting dye concentration (5−20 ppm) and the photodegradation efficiency were studied to be correlated, as shown in Figure 7. As the MB dye solution concentration was initially less than 15 ppm, the photodegradation efficiency of TiO_2/CuO did not significantly alter. This demonstrated that even at low concentrations of the MB dye, TiO_2/CuO maintained a steady catalytic function. The photocatalytic efficiency of TiO_2/CuO NC decreased gradually as the starting concentration of the MB solution was increased; similar outcomes were observed for the photocatalytic degradation of other dyes. The TiO_2/CuO NC degradation efficiency was 73% when the initial concentration of MB was 5 ppm. When the dye concentration was increased to 15 ppm, the degradation efficiency was slightly decreased to 67%. The degradation efficiency significantly decreased as the dye concentration increased to 20 ppm. This is due to the substrate's potent light absorption in the catalyst's excited wavelength region, which could lower the catalytic efficiency. The amount of dye adsorbed on the surfaces of the catalysts increases with an initial concentration of the dye, which prevents the catalyst from absorbing photons to form holes and electrons and decreases the degradation efficiency.[58]

3.6.3. Effect of pH. When assessing the photocatalytic degradation efficiency of MB aqueous solution, pH is a crucial aspect to consider. Since pH can also affect the surface charge of TiO_2/CuO NC, the influence of pH was also investigated in

https://doi.org/10.1021/acsomega.4c03472
ACS Omega 2024, 9, 41301−41313

the pH range of 5−10. As Figure 8 illustrates, a pH value of 9 was found to be the optimum for MB degradation under the TiO_2/CuO NC catalyst. Since the MB dye is a cationic dye, it requires a pH of dispersion that is in the basic range of the photocatalyst. The removal gradually declined once more at pH values greater than 9. This could be because the TiO_2/CuO NC surface's strong negative charge was protonated, losing its negatively charged surface property and decreasing the adsorbing cationic dye feature.[59,60]

3.6.4. Effect of Reaction Time. The percentage of MB photocatalytic degradation on the TiO_2/CuO NC surface is equivalent to the time duration of the reaction time. Figure 9A represents the effect of contact time on the photocatalytic removal of MB at optimized conditions (20 mg of TiO_2/CuO, 15 ppm of MB, at pH 9) in an aqueous solution. The result shows that the rapid photodegradation removal efficiency of MB using the TiO_2/CuO catalyst was approximately 99% after an irradiation time duration of 90 min. It was found that as the time of light irradiation prolonged, the percentage of photodegradation efficiency increased and reached a maximum after 90 min. Figure 9B,9C shows the photodegradation efficiency of the pristine TiO_2 and CuO, respectively, at the optimized conditions of their nanocomposite (TiO_2/CuO NC). Figure 9D shows the photodegradation efficiencies versus time plot of TiO_2/CuO, TiO_2, and CuO.

The reaction kinetics of the photocatalytic degradation activity was studied by plotting ln(Co/C) vs time for pseudo-first-order as shown in Figure 9E. It was also investigated for pseudo-second-order reaction kinetics as indicated in Figure 9F. The linear fitted straight line's slope indicates the photodegradation rate; nanomaterials with a high slope revealed a high photodegradation efficiency. The TiO_2/CuO NC demonstrated both the highest slope and the highest removal efficiency for MB in both pseudo-first and pseudo-second order, with the TiO_2/CuO NC enabling almost complete removal of MB in just 90 min as compared to the pristine TiO_2 and CuO NPs. Table 1 summarizes the rate constant, efficiency, and regression coefficient over 90 min. The TiO_2/CuO nanocomposite synthesized in this work showed good performance compared with reported works as shown in Table 2.[61,62]

Table 1. Quantitative Analysis of the Rate Constant, Regression, and Photocatalytic Efficiency of the Biosynthesized Nanomaterials at Optimized Conditions

biosynthesized materials		TiO_2/CuO	TiO_2	CuO
rate constant	pseudo 1st order (min^{-1})	0.033	0.017	0.011
	pseudo 2nd order (ppm min^{-1})	0.025	0.02	0.013
regression (R^2)	pseudo 1st order	0.995	0.993	0.991
	pseudo 2nd order	0.873	0.765	0.761
photodegradation efficiency		99	73	60

3.7. Reusability Test. For the reusability test of TiO_2, CuO, and TiO_2/CuO nanomaterials on the photodegradation of the MB dye, five cycles of the degradation process were carried out at the optimized conditions (15 ppm dye, at pH9 for 90 min) and the results are shown in Figure 10 and summarized in Table 2. The catalysts were collected by centrifuging them after each round of photocatalytic degradation, cleaned with a solution of distilled water and ethanol, and then dried in a hot air microwave oven. The samples were utilized once again for the dye's photocatalytic degradation. The dye concentration, catalyst dose, pH, and time were all maintained at the same levels at their optimum value.

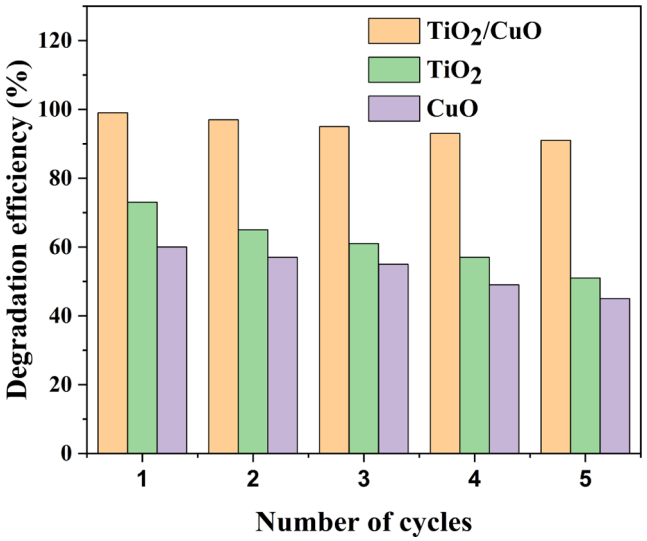

Figure 10. Recyclability test of TiO_2/CuO, TiO_2, and CuO nanomaterials on the photodegradation of the MB dye.

3.8. Scavenging Tests. The rate of degradation processes is significantly impacted by the concentration of reactive oxygen species (ROS) hitting the target molecules. Before irradiating the reaction mixture, several sacrificial reagents were added to trap these species and determine which one was more responsible for the photodegradation of the MB. This allowed us to study the influence of photogenerated electrons, holes, $OH^•$, and $O_2^{•-}$ radicals on the photodegradation of the MB.[63] Ethylenediaminetetraacetic acid disodium (EDTA-2Na) as an h^+ scavenger,[64] isopropanol (IPA) as an $OH^•$ scavenger,[65] silver nitrate ($AgNO_3$) as an e^- scavenger,[66] and acetonitrile as an $O_2^{•-}$ scavenger were used.[67,68]

It is shown in Table 3 and Figure 11 that the photodegradation efficiency in the presence of reactive species scavengers is in the order of EDTA-2Na (41%) < $AgNO_3$ (56%) < ACN (68%) < IPA (88%) for TiO_2/CuO EDTA-2Na (35%) < $AgNO_3$ (43%) < ACN (54%) < IPA (61%) for TiO_2

Table 2

plant	catalyst	catalyst dose (mg)	MB dye concentration (ppm)	degradation time (min)	efficiency (%)	references
Citrus aurantium juice extract	TiO_2/CuO	93	15	90	98.8	61
Commelina benghalensis	TiO_2/CuO	30	20	120	94	62
I. tinctoria A.rich. leaf extract	TiO_2/CuO	20	15	90	99	this work
I. tinctoria A.rich. leaf extract	TiO_2	20	15	90	73	this work
I. tinctoria A.rich. leaf extract	CuO	20	15	90	60	this work

https://doi.org/10.1021/acsomega.4c03472
ACS Omega 2024, 9, 41301−41313

Table 3. Summary of the Effect of Scavengers on the Photodegradation Efficiency of the MB

	photocatalytic activity		
scavenger	TiO_2/CuO	TiO_2	CuO
no scavenger	99	73	60
IPA	88	61	36
ACN	68	54	47
$AgNO_3$	56	43	31
EDTA-2Na	41	35	49

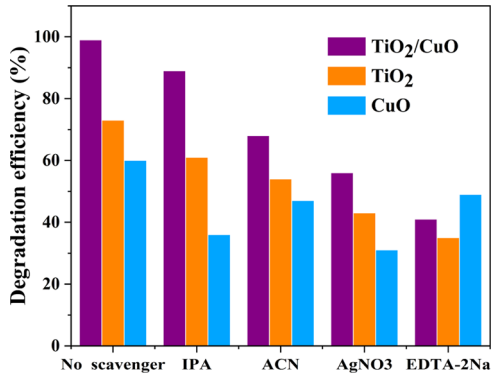

Figure 11. Effect of radical scavengers on the photocatalytic ability of TiO_2, CuO, and TiO_2/CuO.

and $AgNO_3$ (31%) < IPA (36%) < ACN (47%) < EDTA-2Na (49%) for CuO. This shows that h^+ has the highest contribution to the photocatalytic activity of both TiO_2/CuO and TiO_2 whereas e^- plays a great role in the photocatalytic degradation activity of CuO.[69]

4. CONCLUSIONS

The green method by the extract of *I. tinctoria* A.Rich leaves was effectively used to synthesize TiO_2, CuO, and TiO_2/CuO nanomaterials. The PL analysis showed that there was electron−hole recombination hindrance in the TiO_2/CuO NC compared to the pristine TiO_2 and CuO NPs. From the XRD analysis of TiO_2/CuO, the average crystallite size was found to be 21 nm. The HRTEM study confirmed that the TiO_2/CuO composite was in close contact; the *d*-spacing values of 0.352 and 0.19 nm, respectively, matched the (101) and (200) crystal planes of the TiO_2 anatase phase. The *d*-spacing values of 0.213 and 0.252 nm correspond to the crystal planes of (111) and (11$\bar{1}$), respectively, belonging to the monoclinic CuO. The BET analysis showed the formation of mesoporous TiO_2/CuO with a surface area of 87.5 m^2/g. The biosynthesized TiO_2, CuO, and TiO_2/CuO nanostructures were tested for their photocatalytic degradation activity against the potentially hazardous MB dye. Under optimal conditions, the TiO_2/CuO catalyst exhibited the maximum degrading efficiency of 99% and showed better performance compared to the pristine TiO_2(73%) and CuO (60%) NPs. The photodegradation activity of the MB dye in the presence of TiO_2/CuO NC showed pseudo-first-order kinetics with a rate constant of 0.03 min^{-1} and a regression coefficient of 0.995. The reusability test of the photocatalyst revealed promising stability in the removal of pollutants repeatedly. The nanomaterials synthesized in this work will be tested for other applications such as antimicrobial activity, sensors, and electrode materials for solar cell applications.

ASSOCIATED CONTENT

Supporting Information

The Supporting Information is available free of charge at https://pubs.acs.org/doi/10.1021/acsomega.4c03472.

Experimental procedures for the collection of plant; preparation of the plant extract; and phytochemical analysis; extract preparation scheme (Figure S1); possible mechanism of formation of oxides nanomaterials by plant extract synthesis method (Figure S2); probable mechanism of formation methylene blue degradation by TiO_2/CuO NC (Figure S3); and optimization of catalyst dosage, dye concentration, and pH for the pristine TiO_2 and CuO (Figures S4−S9); the phytochemical screening test summary (Table S1) (PDF)

AUTHOR INFORMATION

Corresponding Authors

Dereje Tsegaye Leku − *Department of Applied Chemistry, School of Applied and Natural Sciences, Adama Science and Technology University, 1888 Adama, Ethiopia*; Phone: +251911530922; Email: detsegaye@gmail.com

Getachew Adam Workneh − *Department of Industrial Chemistry, Addis Ababa Science and Technology University, 16417 Addis Ababa, Ethiopia; Sustainable Energy Center of Excellence, Addis Ababa Science and Technology University, 16417 Addis Ababa, Ethiopia*; orcid.org/0000-0002-2863-1379; Phone: +251911162496; Email: getachew.adam@aastu.edu.et.

Authors

Getye Behailu Yitagesu − *Department of Applied Chemistry, School of Applied and Natural Sciences, Adama Science and Technology University, 1888 Adama, Ethiopia*

Abebaw Matebu Seyume − *Department of Industrial Chemistry, Addis Ababa Science and Technology University, 16417 Addis Ababa, Ethiopia; Sustainable Energy Center of Excellence, Addis Ababa Science and Technology University, 16417 Addis Ababa, Ethiopia*

Complete contact information is available at: https://pubs.acs.org/10.1021/acsomega.4c03472

Author Contributions

Writing original draft and laboratory activity by G.B. and A.M. Writing review and editing of the paper was done by G.A. and D.T. All authors read the final manuscript and approved it.

Notes

The authors declare no competing financial interest.

ACKNOWLEDGMENTS

The authors acknowledge Adama Science and Technology University and Wachemo University for their financial support.

REFERENCES

(1) Ali, F.; Mehmood, S.; Ashraf, A.; Saleem, A.; Younas, U.; Ahmad, A.; Bhatti, M. P.; Eldesoky, G. E.; Aljuwayid, A. M.; Habila, M. A.; et al. Ag−Cu Embedded SDS Nanoparticles for Efficient Removal of Toxic Organic Dyes from Water Medium. *Ind. Eng. Chem. Res.* **2023**, *62* (11), 4765−4777.

(2) Ghazy, N. M.; Ghaith, E. A.; El-Reash, Y. G. A.; Zaky, R. R.; El-Maaty, W. M. A.; Awad, F. S. Enhanced performance of hydroxyl and cyano group functionalized graphitic carbon nitride for efficient

removal of crystal violet and methylene blue from wastewater. *RSC Adv.* **2022**, *12* (55), 35587−35597.
(3) Tayade, R. J.; Kulkarni, R. G.; Jasra, R. V. Transition metal ion impregnated mesoporous TiO2 for photocatalytic degradation of organic contaminants in water. *Ind. Eng. Chem. Res.* **2006**, *45* (15), 5231−5238.
(4) Chowdhury, A. P.; Anantharaju, K.; Keshavamurthy, K.; Rokhum, S. L. Recent Advances in Efficient Photocatalytic Degradation Approaches for Azo Dyes. *J. Chem.* **2023**, *2023* (1), No. 9780955.
(5) Ghamari Kargar, P.; Maleki, B.; Ghani, M. Ag/GO/Fe3O4/γ-Fe2O3 Nanocomposite for Green-Light-Driven Photocatalytic Oxidation of 5-Hydroxymethylfurfural to 5-Hydroxymethyl-2-furancarboxylic Acid. *ACS Appl. Nano Mater.* **2024**, *7* (8), 8765−8782.
(6) Alamier, W. M.; DY Oteef, M.; Bakry, A. M.; Hasan, N.; Ismail, K. S.; Awad, F. S. Green Synthesis of Silver Nanoparticles Using Acacia ehrenbergiana Plant Cortex Extract for Efficient Removal of Rhodamine B Cationic Dye from Wastewater and the Evaluation of Antimicrobial Activity. *ACS Omega* **2023**, *8*, 18901−18914, DOI: 10.1021/acsomega.3c01292.
(7) Agarwalla, S.; Kodialbail, V. S. Extracellular biosynthesis of CuO-TiO2 nanocomposites using Alcaligenes aquatilis for the photodegradation of reactive and azo dyes under visible light irradiation *Environ. Sci. Pollut. Res.* 2023 .
(8) Martins, L. R.; Soares, L. C.; Gurgel, L. V. A.; Gil, L. F. Use of a new zwitterionic cellulose derivative for removal of crystal violet and orange II from aqueous solutions. *J. Hazard. Mater.* **2022**, *424*, No. 127401.
(9) Gendo, K. M.; Bogale, R. F.; Kenasa, G. Green Synthesis, Characterization, and Evaluation of Photocatalytic and Antibacterial Activities of Co3O4−ZnO Nanocomposites Using Calpurnia aurea Leaf Extract. *ACS Omega* **2024**, *9*, 28354−28371, DOI: 10.1021/acsomega.4c01595.
(10) Hosseini, H.; Zirakjou, A.; McClements, D. J.; Goodarzi, V.; Chen, W.-H. Removal of methylene blue from wastewater using ternary nanocomposite aerogel systems: Carboxymethyl cellulose grafted by polyacrylic acid and decorated with graphene oxide. *J. Hazard. Mater.* **2022**, *421*, No. 126752.
(11) Salavati, H.; Teimouri, A.; Kazemi, S. Investigation of photocatalytic performance of keggin type heteropolyacid in degradation of methylene blue. *Chem. Methodol.* **2017**, *2*, 158−169.
(12) Ayub, M.; Othman, M. H. D. Graphene Oxide-Based Nanofiltration Membranes for Separation of Heavy Metals. In *Emerging Techniques for Treatment of Toxic Metals from Wastewater*; Elsevier, 2023; pp 231−288.
(13) Shoshaa, R.; Ashfaq, M. Y.; Al-Ghouti, M. A. Recent developments in ultrafiltration membrane technology for the removal of potentially toxic elements, and enhanced antifouling performance: A review. *Environ. Technol. Innovation* **2023**, *31*, No. 103162.
(14) Ali, A.; Sadia, M.; Azeem, M.; Ahmad, M. Z.; Umar, M.; Abbas, Z. U. Ion Exchange Resins and their Applications in Water Treatment and Pollutants Removal from Environment: A Review: Ion Exchange Resins and their Applications. *Futuristic Biotechnol.* **2023**, *3*, 12−19.
(15) Lanjwani, M. F.; Tuzen, M.; Khuhawar, M. Y.; Saleh, T. A. Trends in photocatalytic degradation of organic dye pollutants using nanoparticles: a review. *Inorg. Chem. Commun.* **2024**, *159*, No. 111613.
(16) Bekru, A. G.; Tufa, L. T.; Zelekew, O. A.; Goddati, M.; Lee, J.; Sabir, F. K. Green synthesis of a CuO−ZnO nanocomposite for efficient photodegradation of methylene blue and reduction of 4-nitrophenol. *ACS Omega* **2022**, *7* (35), 30908−30919.
(17) Kargar, P. G.; Maleki, B.; Ghani, M. $Fe_3O_4/Fe_2O_3/TiO_2$/Ag: an innovative photocatalyst under visible light irradiation in deep eutectic solvent for efficient conversion of 5-HMF to chemo-and bio-based chemicals besides their determination using HPLC *Biomass Convers. Biorefin.* 2023.
(18) Pavel, M.; Anastasescu, C.; State, R.-N.; Vasile, A.; Papa, F.; Balint, I. Photocatalytic degradation of organic and inorganic pollutants to harmless end products: assessment of practical application potential for water and air cleaning. *Catalysts* **2023**, *13* (2), No. 380.
(19) Sim, S.; Wong, N. K. Nanotechnology and its use in imaging and drug delivery. *Biomed. Rep.* **2021**, *14* (5), No. 42.
(20) Jeevarathinam, M.; Sivagami, M.; Kuruthukulangara, N.; Ragavi, S.; Thirumalai, D.; Asharani, I. Green Synthesis of Metal/Metal Oxide Nanoparticles and Their Photocatalytic Degradation of Dyes. In *Photocatalysis for Energy and Environmental Applications: Current Trends and Future Perspectives*; Springer, 2024; pp 191−228.
(21) Verma, V.; Al-Dossari, M.; Singh, J.; Rawat, M.; Kordy, M. G.; Shaban, M. A review on green synthesis of TiO2 NPs: photocatalysis and antimicrobial applications. *Polymers* **2022**, *14* (7), No. 1444.
(22) Haleem, A.; Javaid, M.; Singh, R. P.; Rab, S.; Suman, R. Applications of Nanotechnology in Medical field: A brief review. *Global Health J.* **2023**, *7*, 70−77, DOI: 10.1016/j.glohj.2023.02.008.
(23) Sun, Y.; Zhang, W.; Li, Q.; Liu, H.; Wang, X. Preparations and applications of zinc oxide based photocatalytic materials. *Adv. Sens. Energy Mater.* **2023**, *2*, No. 100069.
(24) Pawar, M.; Gaonar, M.; Khajone, A.; Malasane, P. Green Synthesis of Nb2O5 Nanoparticles and Photodegradation of Remazol Yellow RR Dye **2023** *6* 1 9 DOI: 10.36349/easjmb.2023.v06i01.001.
(25) Shabna, S.; Dhas, S. S. J.; Biju, C. Potential progress in SnO2 nanostructures for enhancing photocatalytic degradation of organic pollutants. *Catal. Commun.* **2023**, *177*, No. 106642.
(26) Baral, S. C.; Maneesha, P.; Datta, S.; Dukiya, K.; Sasmal, D.; Samantaray, K. S.; BR, V. K.; Dasgupta, A.; Sen, S. Enhanced photocatalytic degradation of organic pollutants in water using copper oxide (CuO) nanosheets for environmental application. *JCIS Open* **2024**, *13*, No. 100102.
(27) Kusmierek, E. A CeO2 semiconductor as a photocatalytic and photoelectrocatalytic material for the remediation of pollutants in industrial wastewater: a review. *Catalysts* **2020**, *10* (12), No. 1435.
(28) Kamble, G. S.; Natarajan, T. S.; Patil, S. S.; Thomas, M.; Chougale, R. K.; Sanadi, P. D.; Siddharth, U. S.; Ling, Y.-C. BiVO4 as a sustainable and emerging photocatalyst: Synthesis methodologies, engineering properties, and its volatile organic compounds degradation efficiency. *Nanomaterials* **2023**, *13* (9), No. 1528.
(29) Liu, Z.; Yu, X.; Wang, K.; Yu, H.; Wang, T.; Zhao, N.; Zhang, J. Preparation of WO3 Particles and Their Photocatalytic Properties. *J. Phys.: Conf. Ser.* **2023**, *2610*, No. 012055, DOI: 10.1088/1742-6596/2610/1/012055.
(30) Alp, E.; Borazan, İ. The production of highly efficient visible-light-driven electrospun α-Fe2O3 photocatalyst through modifying iron source material for wastewater treatment applications. *J. Chin. Chem. Soc.* **2023**, *70* (7), 1510−1520.
(31) Solymos, K.; Babcsányi, I.; Ariya, B.; Gyulavári, T.; Ágoston, Á.; Szamosvölgyi, Á.; Kukovecz, Á.; Kónya, Z.; Farsang, A.; Pap, Z. Photocatalytic and surface properties of titanium dioxide nanoparticles in soil solutions. *Environ. Sci.: Nano* **2024**, *11*, 1204−1216, DOI: 10.1039/D3EN00622K.
(32) Devia, P.; Singh, J. In *Role of Oxygen Vacancies in* In_2O_3 *Nanostructures towards Enhancement of Photocatalytic Activity*, 2020 5th IEEE International Conference on Emerging Electronics (ICEE); IEEE, 2020; pp 1−4.
(33) Abebe, B.; Zereffa, E. A.; Murthy, H. A. Synthesis of poly (vinyl alcohol)-aided ZnO/Mn2O3 nanocomposites for acid orange-8 dye degradation: mechanism and antibacterial activity. *ACS Omega* **2021**, *6* (1), 954−964.
(34) Kubiak, A.; Siwińska-Ciesielczyk, K.; Goscianska, J.; Dobrowolska, A.; Gabała, E.; Czaczyk, K.; Jesionowski, T. Hydrothermal-assisted synthesis of highly crystalline titania−copper oxide binary systems with enhanced antibacterial properties. *Mater. Sci. Eng.: C* **2019**, *104*, No. 109839.
(35) Araújo, E. S.; Pereira, M. F.; da Silva, G. M.; Tavares, G. F.; Oliveira, C. Y.; Faia, P. M. A Review on the Use of Metal Oxide-Based Nanocomposites for the Remediation of Organics-Contaminated Water via Photocatalysis: Fundamentals, Bibliometric Study and Recent Advances. *Toxics* **2023**, *11* (8), No. 658.

(36) Gan, Y. X.; Jayatissa, A. H.; Yu, Z.; Chen, X.; Li, M. Hydrothermal synthesis of nanomaterials. *J. Nanomater.* **2020**, *2020*, 1−3.
(37) Mekuye, B.; Abera, B. Nanomaterials: An overview of synthesis, classification, characterization, and applications. *Nano Select* **2023**, *4*, 486−501, DOI: 10.1002/nano.202300038.
(38) Ijaz, I.; Gilani, E.; Nazir, A.; Bukhari, A. Detail review on chemical, physical and green synthesis, classification, characterizations and applications of nanoparticles. *Green Chem. Lett. Rev.* **2020**, *13* (3), 223−245.
(39) Khan, N.; Ali, S.; Latif, S.; Mehmood, A. Biological synthesis of nanoparticles and their applications in sustainable agriculture production. *Nat. Sci.* **2022**, *14* (6), 226−234.
(40) Singh, H.; Desimone, M. F.; Pandya, S.; Jasani, S.; George, N.; Adnan, M.; Aldarhami, A.; Bazaid, A. S.; Alderhami, S. A. Revisiting the green synthesis of nanoparticles: uncovering influences of plant extracts as reducing agents for enhanced synthesis efficiency and its biomedical applications. *Int. J. Nanomed.* **2023**, *18*, 4727−4750.
(41) Singh, A.; Gautam, P. K.; Verma, A.; Singh, V.; Shivapriya, P. M.; Shivalkar, S.; Sahoo, A. K.; Samanta, S. K. Green synthesis of metallic nanoparticles as effective alternatives to treat antibiotics resistant bacterial infections: A review. *Biotechnol. Rep.* **2020**, *25*, No. e00427.
(42) Abdelbaky, A. S.; Mohamed, A. M.; Sharaky, M.; Mohamed, N. A.; Diab, Y. M. Green approach for the synthesis of ZnO nanoparticles using Cymbopogon citratus aqueous leaf extract: characterization and evaluation of their biological activities. *Chem. Biol. Technol. Agric.* **2023**, *10* (1), No. 63.
(43) Gidamo, G. H. Antioxidant activity and mineral content of Impatiens tinctoria A. Rich (Ensosila) tuber, an Ethiopian medicinal plant. *Sci. Rep.* **2023**, *13* (1), No. 14998.
(44) Molole, G. J.; Gure, A.; Abdissa, N. Determination of total phenolic content and antioxidant activity of Commiphora mollis (Oliv.) Engl. resin. *BMC Chem.* **2022**, *16* (1), No. 48.
(45) Degu, S.; Gemeda, N.; Abebe, A.; Berihun, A.; Debebe, E.; Sisay, B.; Gemeda, H.; Ashebir, R.; Amano, A.; Fekadu, N. In vitro antifungal activity, phytochemical screening and thin layer chromatography profiling of Impatiens tinctoria A. Rich root extracts. *J. Med. Plants Stud.* **2020**, *8*, 189−196.
(46) Basit, R. A.; Abbasi, Z.; Hafeez, M.; Ahmad, P.; Khan, J.; Khandaker, M. U.; Al-Mugren, K. S.; Khalid, A. Successive photocatalytic degradation of methylene blue by ZnO, CuO and ZnO/CuO synthesized from coriandrum sativum plant extract via green synthesis technique. *Crystals* **2023**, *13* (2), No. 281.
(47) Gou, X.; Guo, Z. Hybrid hydrophilic−hydrophobic CuO@ TiO2-coated copper mesh for efficient water harvesting. *Langmuir* **2020**, *36* (1), 64−73.
(48) Ramírez, S. P.; Wang, J.; Valenzuela, M.; Chen, L.; Dalai, A. CuO@ TiO2 and NiO@ TiO2 core-shell catalysts for hydrogen production from the photocatalytic reforming of glycerol aqueous solution. *J. Appl. Res. Technol.* **2020**, *18* (6), 390−409.
(49) Makuła, P.; Pacia, M.; Macyk, W. How to correctly determine the band gap energy of modified semiconductor photocatalysts based on UV−Vis spectra. *The J. Phys. Chem. Lett.* **2018**, *9*, 6814−6817, DOI: 10.1021/acs.jpclett.8b02892.
(50) Zhao, L.; Cui, T.; Li, Y.; Wang, B.; Han, J.; Han, L.; Liu, Z. Efficient visible light photocatalytic activity of p−n junction CuO/TiO 2 loaded on natural zeolite. *RSC Adv.* **2015**, *5* (79), 64495−64502.
(51) Abbood, H. K.; Ali, N. A. Studying of the structural and optical properties of titanium dioxide nanoparticles prepared by chemical method. *J. Opt.* **2023**, *53*, 2698−2703.
(52) Shawky, A. M.; Elshypany, R.; El Sharkawy, H. M.; Mubarak, M. F.; Selim, H. Emerald eco-synthesis: harnessing oleander for green silver nanoparticle production and advancing photocatalytic MB degradation with TiO2&CuO nanocomposite. *Sci. Rep.* **2024**, *14* (1), No. 2456.
(53) Sethy, N. K.; Arif, Z.; Mishra, P. K.; Kumar, P. Green synthesis of TiO2 nanoparticles from Syzygium cumini extract for photocatalytic removal of lead (Pb) in explosive industrial wastewater. *Green Process. Synth.* **2020**, *9* (1), 171−181.
(54) Sayed, M. Y. E.; Ghouch, N. E.; Younes, G.; Noun, M.; Awad, R.Tailoring the Structural, Optical and Anti-corrosion Effect of Synthesized Sn-Doped CuO Nanoparticles on Mild Steel in 0.5 M HCl Solution *J. Mater. Eng. Perform.* 2024 .
(55) Baloguna, S.; Oyesholab, H.; Belloa, S.; Ojoa, S. Ixora Coccinea Extract for Biosynthesis of Titanium Dioxide Nanoparticles: A Precursor for Organic Electronics. *J. Mater.* **2024**, *2* (4), 279−287.
(56) Subha, P. P.; Vikas, L.; Jayaraj, M. Solution-processed CuO/TiO2 heterojunction for enhanced room temperature ethanol sensing applications. *Phys. Scr.* **2018**, *93* (5), No. 055001.
(57) Mortazavian, S.; Saber, A.; James, D. E. Optimization of photocatalytic degradation of acid blue 113 and acid red 88 textile dyes in a UV-C/TiO2 suspension system: application of response surface methodology (RSM). *Catalysts* **2019**, *9* (4), No. 360.
(58) Zhang, D.; Lv, S.; Luo, Z. A study on the photocatalytic degradation performance of a [KNbO 3] 0.9-[BaNi 0.5 Nb 0.5 O 3−*δ*] 0.1 perovskite. *RSC Adv.* **2020**, *10* (3), 1275−1280.
(59) Reza, K. M.; Kurny, A.; Gulshan, F. Parameters affecting the photocatalytic degradation of dyes using TiO 2: a review. *Appl. Water Sci.* **2017**, *7*, 1569−1578.
(60) Chaudhari, S. M.; Gawal, P. M.; Sane, P. K.; Sontakke, S. M.; Nemade, P. R. Solar light-assisted photocatalytic degradation of methylene blue with Mo/TiO 2: A comparison with Cr-and Ni-doped TiO 2. *Res. Chem. Intermed.* **2018**, *44*, 3115−3134.
(61) Bassim, S.; Mageed, A. K.; AbdulRazak, A. A.; Al-Sheikh, F. Photodegradation of methylene blue with aid of green synthesis of CuO/TiO2 nanoparticles from extract of citrus aurantium juice. *Bull. Chem. React. Eng. Catal.* **2023**, *18* (1), 1−16.
(62) Bopape, D. A.; Mathobela, S.; Matinise, N.; Motaung, D. E.; Hintsho-Mbita, N. C. Green synthesis of CuO-TiO2 nanoparticles for the degradation of organic pollutants: physical, optical and electrochemical properties. *Catalysts* **2023**, *13* (1), No. 163.
(63) Mugumo, R.; Ichipi, E.; Tichapondwa, S. M.; Chirwa, E. M. N. Visible-Light-Induced Photocatalytic Degradation of Rhodamine B Dye Using CuS/ZnS PN Heterojunction Nanocomposite under Visible Light Irradiation. *Catalysts* **2023**, *13*, No. 1184, DOI: 10.3390/catal13081184.
(64) Bakry, A. M.; Alamier, W. M.; El-Shall, M. S.; Awad, F. S. Facile synthesis of amorphous zirconium phosphate graphitic carbon nitride composite and its high performance for photocatalytic degradation of indigo carmine dye in water. *J. Mater. Res. Technol.* **2022**, *20*, 1456−1469.
(65) Salesi, S.; Nezamzadeh-Ejhieh, A. An experimental design study of photocatalytic activity of the Z-scheme silver iodide/tungstate binary nano photocatalyst. *Environ. Sci. Pollut. Res.* **2023**, *30*, 105440−105456.
(66) Yitagesu, G. B.; Leku, D. T.; Workneh, G. A. Green Synthesis of TiO2 Using Impatiens rothii Hook. f. Leaf Extract for Efficient Removal of Methylene Blue Dye. *ACS Omega* **2023**, *8*, 43999−44012, DOI: 10.1021/acsomega.3c06142.
(67) Saharudin, K. A.; Sreekantan, S.; Basiron, N.; Khor, Y. L.; Harun, N. H.; SMN Mydin, R. B.; Md Akil, H.; Seeni, A.; Vignesh, K. Bacteriostatic Activity of LLDPE Nanocomposite Embedded with Sol−Gel Synthesized TiO2/ZnO Coupled Oxides at Various Ratios. *Polymers* **2018**, *10* (8), No. 878.
(68) Gadore, V.; Singh, A. K.; Mishra, S. R.; Ahmaruzzaman, M. RSM approach for process optimization of the photodegradation of congo red by a novel NiCo2S4/chitosan photocatalyst. *Sci. Rep.* **2024**, *14* (1), No. 1184.
(69) Sharma, S.; Kumar, N.; Mari, B.; Chauhan, N. S.; Mittal, A.; Maken, S.; Kumari, K. Solution combustion synthesized TiO2/Bi2O3/CuO nano-composites and their photocatalytic activity using visible LEDs assisted photoreactor. *Inorg. Chem. Commun.* **2021**, *125*, No. 108418.